JACS
JOURNAL OF THE AMERICAN CHEMICAL SOCIETY

Article

pubs.acs.org/JACS

Crystallization of Keggin Heteropolyanions via a Two-Step Process in Aqueous Solutions

Mrinal K. Bera*,† and Mark R. Antonio*

Chemical Sciences and Engineering Division, Argonne National Laboratory, Argonne, Illinois 60439, United States

Supporting Information

ABSTRACT: Although the analytical simplicity of the one-step classical theory of nucleation facilitates its use to understand crystallization processes, recent experiments and simulations have shown that many occur via multiple steps. According to the contemporary two-stage theory of nucleation, the onset of crystallization in a solution is preceded by large density fluctuations in the mother liquor that results in the formation of dense liquid-like correlated structures of the constituent solute particles. Here we report the observation of dense liquid-like correlated structures of heteropolyacid salts of α-Keggin anions (heteropolyanions) in aqueous solutions as volume is decreased long before the onset of crystallization by in situ time-dependent small-angle X-ray scattering measurements. Experiments were performed on drying drops of solutions of heteropolyacids to monitor their ordering before and during the onset of their crystallization. A continuous change in the density of the correlated structures is observed up to the onset of crystallization. Moreover, the correlated structures and the onset of crystallization are found to depend upon the charge of the heteropolyanions. The crystals formed within the drying drops of solutions during the crystallization process are found to be metastable polymorphic structures that are different from the stable crystal structures obtained after complete drying of the drops. Our results support a two-step process and Ostwald's rule of stages for the crystallization of heteropolyanions in their aqueous solutions upon evaporation.

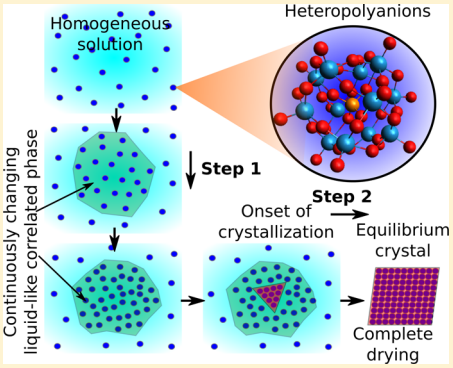

INTRODUCTION

The formation of crystals in solutions is a subject of long-standing research in a number of diverse fields, especially chemistry,[1] biology,[2] medicine,[3] and material sciences.[4−6] It is very well-known that when a solution approaches a critical concentration, which is known as the saturation condition, the solutes start to separate out of the solution in the form of crystals.[6−11] Although crystallization is widely used and known for centuries, a basic understanding of the nucleation process of crystallization is still in its infancy. The earliest known thermodynamic understanding of crystallization was put forward by Gibbs who framed the phenomenon in terms of a one-step nucleation process. This is popularly known today as classical nucleation theory (CNT).[12] But subsequent experiments[6,13−17] and computer simulations[18,19] throughout the last two decades have shown evidence for multiple-step processes and support the picture put forward by Ostwald that is popularly known as the Ostwald rule of stages.[20] For instance, Chung et al.,[14] while studying the crystallization of amorphous $LiFePO_4$ at 450 °C using transmission electron microscopy, have recently shown evidence of transformations through multiple metastable crystalline phases before reaching the stable crystalline phase. Also Chowdhury et al.[13] have shown, using second harmonic generation microscopy, the formation of metastable polymorphs of amino acids during their crystallization by rapid evaporation. Working with aqueous colloidal suspensions, Zhang et al.[17,21] found that crystallization driven by alternating electric fields occurs through metastable liquid-like structures. In general, the presence of a metastable liquid-like phase before the onset of crystallization is typical of a two-step process. In the first step, a liquid-like nucleus emerges out of the homogeneous solution; in the second one, the liquid transforms through a series of metastable crystalline phases. Apart from the aforementioned studies that are mainly based on structural analysis of in situ crystallization, researchers have developed another technique that uses the sensitivity of catalytic hydrogenation reactions to probe the growth of nanoparticles.[1,22−24] Even in the absence of structural information, the method has revealed definitive insights into the two-kinetic-step mechanism for the formation of nanoparticles from their precursor solutions. The first and rate-limiting step was clearly attributed to the slow-continuous-homogeneous nucleation of reduced metal atoms, whereas the second and fast step was shown to involve autocatalytic surface growth.[1,22−24]

Besides experimental research, recent advancements in computational techniques have provided evidence that crystallization proceeds through multiple metastable stages rather than the one-step CNT.[19,25−27] Nonetheless, there is still sound materials science research today on magnetic materials[28] showing that crystallization occurs in a one-step process in

Received: December 22, 2015
Published: June 1, 2016

DOI: 10.1021/jacs.5b13375
J. Am. Chem. Soc. 2016, 138, 7282−7288

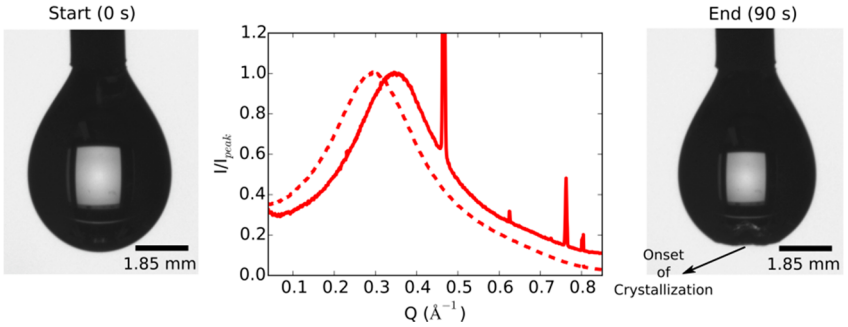

Figure 1. SAXS data and images of the pendant drop of the 0.4 M solution of $H_3PW_{12}O_{40}$ in 0.1 M HCl at the beginning (left image and red dashed line) and at the instant that crystals are observed at the bottom of the drop (right image and red solid line). Crystal formation is revealed by the appearance of a series of sharp Bragg peaks in the SAXS data, which are normalized by the intensities of the broad peaks corresponding to the long-range correlations between heteropolyanions. The flat-surface-like appearance at the bottom of the pendant drop in the rightmost image reveals the presence of solid crystalline precipitates.

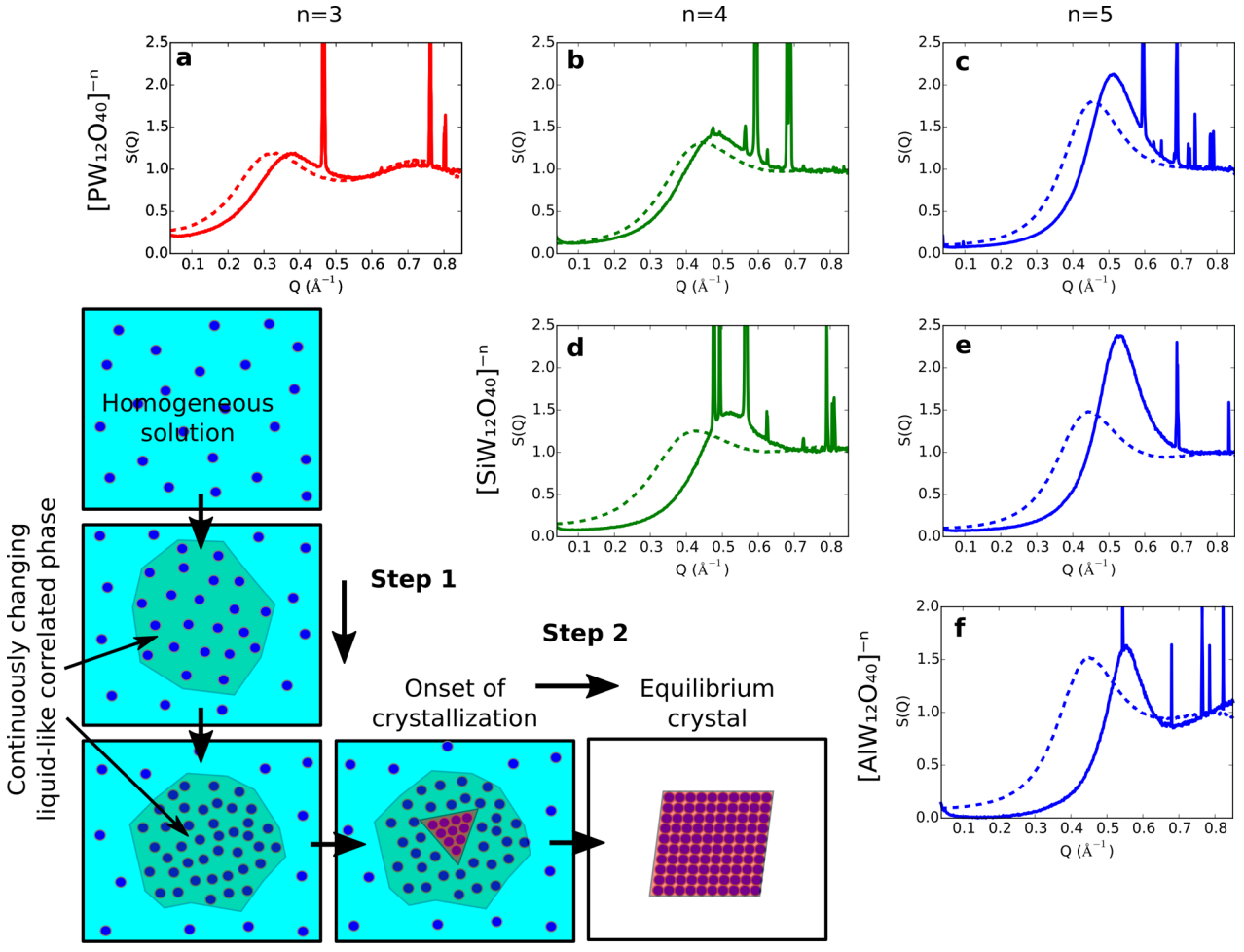

Figure 2. Structure factors, $S(Q)$, extracted from the experimental SAXS data obtained from pendant drops of the 0.4 M solutions of $[PW_{12}O_{40}]^{n-}$ for (a) $n = 3$, (b) $n = 4$, and (c) $n = 5$. Structure factors for the pendant drops of the 0.4 M solutions of $[SiW_{12}O_{40}]^{n-}$ for (d) $n = 4$ and (e) $n = 5$. (f) Structure factors for the pendant drop of the 0.4 M solution of $[AlW_{12}O_{40}]^{n-}$ for $n = 5$. In each of the graphs, the dashed lines correspond to the data collected at the start when the drops were first formed; the solid lines correspond to the data collected at the instant of crystallization. The solid crystals provide the sharp peaks that appear with the broad correlation peaks attributable to the solution structure. A schematic of the crystallization of HPAs via a two-step process is shown in the lower left side of the figure where the HPAs are denoted by dark blue spheres. The process starts with the formation of a dense liquid-like correlated phase from the homogeneous solution. This correlated liquid phase, which is highlighted with a light green background, evolves with time before the onset of crystallization. This is the first step of the two-step process. At the onset of crystallization as depicted inside the magenta triangle, crystals start forming within the dense liquid phase. The transformation goes through a series of polymorphic transitions up to the thermodynamic end point at which the equilibrium crystal structure is obtained after complete drying of the solvent. The formation of metastable crystals within the dense liquid is the second step of the process.

DOI: 10.1021/jacs.5b13375
J. Am. Chem. Soc. 2016, 138, 7282−7288

accordance with CNT. Despite the differing and oftentimes confusing interpretations, the general understanding of the kinetics and mechanisms of phase transitions, such as it stands now,[29] is a two-step process.

Because of experimental limitations of sensitivities and detection limits, many of the crystallization measurements done so far have involved either big colloids or proteins. As mentioned beforehand, both have shown evidence of two-step processes. Only recently have experiments[4] on crystallization processes of inorganic salts been shown to support Ostwald's rule of stages. But, remarkably, there are only a few experiments that show the early stages of nucleation of inorganic ions before the formation of metastable crystalline phases. Among the few is a recent in situ TEM study[5] of the formation of $CaCO_3$ crystals in flow-mixed electrolyte solutions that developed dense amorphous (liquid-like) structures just preceding the crystallization of various intermediate structures; behaviors that support Ostwald's rule of stages. By comparison, there are numerous molecular dynamics simulations[18,19,27] reported in this context that support the two-step process for inorganic ions. Experimental studies of nucleation processes in solutions are difficult because the measurements involve the contact of solutions with solid surfaces that can activate heterogeneous processes at the solid−liquid contacts.[30] Herein, by use of a pendant-drop method and small-angle X-ray scattering (SAXS), we avoided such contacts and report the early stages of the growth of Keggin-type heteropolyanions (HPAs) within drops of bulk aqueous solutions suspended from a needle.

Keggin-type HPAs are obtained by dissolving their acid salts (e.g., 12-phosphotungstic acid, also known as 12-tungstophosphoric acid, $H_3PW_{12}O_{40}$, is an archetype heteropolyacid) in water. They are well-known for their Brønsted acidities and redox behaviors.[31] These properties are exploited in numerous applications related to catalysis, fuel cells, and energy storage devices.[32−34] In addition, HPAs have attracted interest due to their self-assembling behaviors in dilute solutions leading to the formation of spherical-shell-like structures that are popularly known as "blackberries".[35,36] Although the self-assembling behaviors of HPAs are not fully understood,[37] strong associations of HPAs with counterions (in the form of protons or other cations) are believed to be the basis of the organization.[38,39] In a recent study[40] on the aggregation of acid salts of Keggin HPAs in dilute aqueous solutions, we have shown that HPAs interact via short-range attractions and long-range repulsions (SALR) similar to the interactions exhibited by charged colloids and proteins in solutions. The short-range attractions are due to the hydrogen-bonding interactions with protons (i.e., H_3O^+) and water molecules, whereas the long-range repulsions are due to screened columbic repulsions. The self-assembling properties in combination with uniform nanometer-scale morphologies and charge distributions as well as SALR-type interactions make HPAs perfect model systems[36] for experimental studies of incipient crystallization. We have conducted solution experiments in a manner that has not been realized beforehand with three Keggin acid salts: $H_3PW_{12}O_{40}$, $H_4SiW_{12}O_{40}$, and $H_5AlW_{12}O_{40}$ that fully dissociate into $PW_{12}O_{40}^{3-}$ (abbreviated P-HPA^{3-}), $SiW_{12}O_{40}^{4-}$ (Si-HPA^{4-}), $AlW_{12}O_{40}^{5-}$ (Al-HPA^{5-}), and protons (H_3O^+).

RESULTS AND DISCUSSION

SAXS data collected from a drop of a P-HPA^{3-} solution at the start (i.e., at the instant of formation of the pendant drop) and at the end (i.e., at the first instant of crystal formation in the drop) of the time-dependent acquisition are shown in Figure 1 (center panel). The data collected in between times are not presented for clarity but are shown in Figure S2a in the SI. The corresponding images of the pendant drops at the initial and final times are also shown in Figure 1 as the left and right panels, respectively. Note the presence of the broad correlation peak at 0.30 Å^{-1} in the initial SAXS data. This peak shifts in a monotonic fashion with time to the higher Q value of 0.35 Å^{-1} at which point the appearance of sharp Bragg peaks is noted (Figure 1). The presence of the broad peak in the initial SAXS data is diagnostic of the formation of liquid-like correlated structures of HPAs in aqueous solution as volume is decreased long before reaching the onset of crystallization. In the final stages of acquisition, the presence of sharp Bragg peaks along with the broad correlation peak indicates the coexistence of crystalline and liquid-like correlated phases, respectively, of P-HPA^{3-}. At the instant at which the sharp peaks first appear in the SAXS data, the image of the drop (Figure 1, right) shows evidence for the accumulation of crystals at the bottom of the drop. In order to gain structural insights into the collective behaviors of each of the HPAs, the structure factors, $S(Q)$, were extracted from the primary experimental data and are shown in Figure 2.

From the data shown in Figure 2, the behaviors of the native P-HPA^{3-}, Si-HPA^{4-}, and Al-HPA^{5-} systems as well as the one- and two-electron-reduced HPAs in aqueous solutions, where protons (i.e., H_3O^+) are the only counter-cations, near the onset of crystallization can be summarized in five points:

(1) Each of the Keggin HPAs show broad correlation peaks in their solutions well before the onset of crystallization. This indicates the formation of liquid-like correlated structures for all three HPA systems.

(2) The P-HPA system with a −3 charge shows two correlation peaks in the structure factors of Figure 2a compared to only one correlation peak for the singly reduced P-HPA and Si-HPA systems with −4 charges and for the doubly reduced P-HPA, singly reduced Si-HPA, and Al-HPA systems with −5 charges (Figure 2b−f). The two correlation peaks are a signature of the formation of percolated monomers of P-HPA^{3-} that form due to short-range attractions and long-range repulsions between the ions.[40] The high-Q correlation peak at 0.73 Å^{-1} for the $H_3PW_{12}O_{40}$ solution indicates that the P-HPAs are touching each other in their percolated structures. Due to stronger electrostatic repulsions between HPAs with −4 and −5 charges, they do not form percolated structures (as found for P-HPA^{3-}) and, as a result, reveal only one correlation peak in the SAXS patterns.

(3) The correlated structures change as a function of time due to solvent evaporation. This corresponds directly with the increase in concentration of the HPAs for which the correlation peaks monotonically shift to higher-Q values with increasing time until saturated solution conditions are attained.

(4) At the point of saturation, all the HPA data show characteristically sharp Bragg peaks along with the broad, liquid-like correlation peaks. The presence of the Bragg peaks indicates the formation of crystals in the solutions.

(5) During the crystal formation phase, the broad correlation peaks stay fixed while the peak intensities gradually decrease with time (refer to Figure S3 in the SI). The

DOI: 10.1021/jacs.5b13375
J. Am. Chem. Soc. 2016, 138, 7282−7288

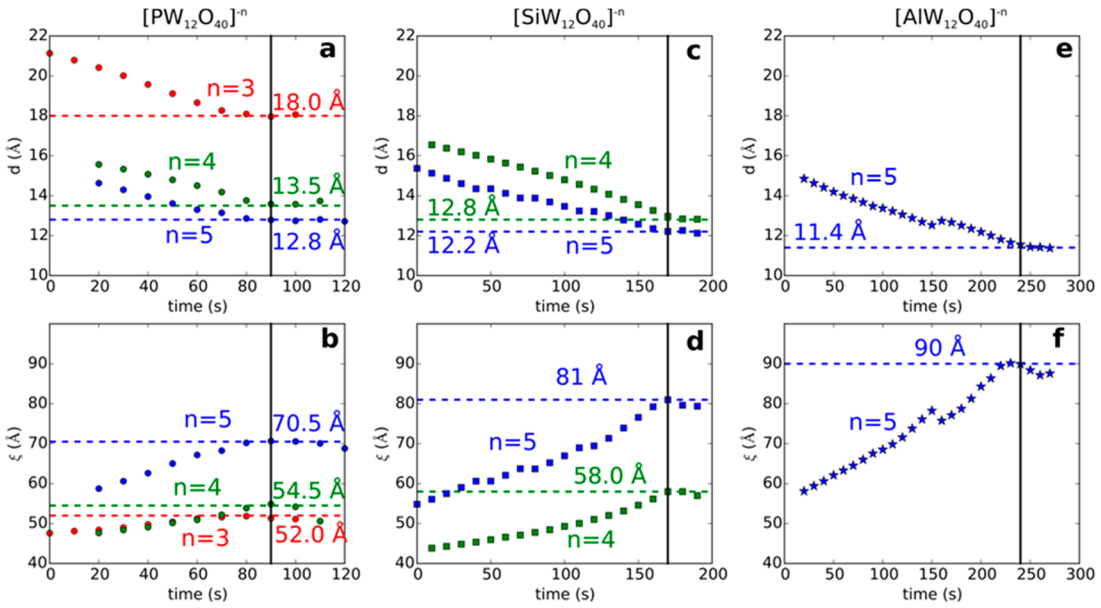

Figure 3. Average HPA–HPA separations (a, c, and e) and correlation lengths (b, d, and f) calculated from the broad correlation peaks of the SAXS patterns obtained as a function of time from pendant drops of 0.4 M solutions of $[PW_{12}O_{40}]^{n-}$, $[SiW_{12}O_{40}]^{n-}$, and $[AlW_{12}O_{40}]^{n-}$ with different values of n as shown in the graphs. With the exception of the Al-HPA^{5-} system, all the data demonstrate smooth evolutions from large, loose aggregates to small, compact ones with time (i.e., water evaporation). The minor discontinuities in the separations (d) and correlation lengths (ξ) seen for $[AlW_{12}O_{40}]^{5-}$ (e and f) are due to the addition of solution to the drop to keep its size the same as the starting size. The addition of solution affects the concentration and, hence, results in small perturbations of both d and ξ at approximately 150 s. Nonetheless, the general trends are identical to those that characterize the P-HPA^{n-} and Si-HPA^{n-} interactions.

fixed-Q correlation peaks suggest that the crystallization process happens at a fixed saturation concentration and that the correlated liquid phase coexists with the newly formed crystalline phases. The decrease in correlation peak intensities suggests the decrease of correlated liquid phases as more and more HPA crystals form and precipitate in the drop.

In order to understand the formation of liquid-like correlated structures of the HPAs before the onset of crystallization, the average HPA–HPA separations (d) and the correlation lengths (ξ) are obtained from the positions (Q_p) and widths (w_p) of the broad correlation peaks as a function of time by using $2\pi/Q_p$ and $2\pi/w_p$, respectively. The results are shown in Figure 3. The general trend observed for all the liquid-like correlated structures is the monotonic decrease and increase in the values of d and ξ, respectively, as a function of time until both of them level off at time-independent values. The time at which they attain constant values is the instant of the onset of crystallization; at this moment, the sharp Bragg peaks make their first appearance. With the increase in magnitude of HPA charge (from −3 to −4 to −5), the values of d and ξ at the onset of crystallization decrease and increase, respectively (see Figure 3). In addition, the values of d and ξ differ for HPAs with the same charge (e.g., P-HPA^{4-} and Si-HPA^{4-}; P-HPA^{5-}, Si-HPA^{5-}, and Al-HPA^{5-}). For instance, the values of d and ξ for singly reduced P-HPA^{4-} (13.5 and 54.5 Å, respectively, in Figure 3a,b) are slightly larger and shorter, respectively, than those for Si-HPA^{4-} (12.8 and 58.0 Å in Figure 3c,d) in its native (i.e., fully oxidized) form. The same trend of decreasing d and increasing ξ with time is also observed for doubly reduced P-HPA^{5-}, singly reduced Si-HPA^{5-}, and Al-HPA^{5-} in its native form. The values of d and ξ at the onset of crystallization for the reduced HPAs lie in between the values for the native ones. For instance, the values of d and ξ are, in order, 13.5 and 54.5 Å for P-HPA^{4-}, 18 and 52.0 Å for P-HPA^{3-} (Figure 3a,b), and 12.8 and 58.0 Å Si-HPA^{4-}. A similar trend is observed for the reduced Si-HPA^{5-} in which the values of d and ξ are 12.2 and 81 Å (Figure 3c,d) compared to the values for Si-HPA^{4-} and 11.4 and 90 Å for Al-HPA^{5-} (Figure 3e,f). We attribute the trend to a slight and uncontrolled oxidation of the reduced HPAs because, during the measurements, the drop was exposed to ambient conditions and to the X-rays. For the correlated structures at the onset of crystallization, with the increase in the magnitude of the HPA charge, the correlation between the HPAs increases as reflected by the reduction of average HPA–HPA separations (d) and the increase in correlation lengths (ξ).

Another aspect that comes out from this study is the time required to reach the onset of crystallization. It is clear from Figure 3 that although we started with equivalent concentrations (approximately 0.4 M) for all the HPAs (native and reduced alike), the time required to reach the onset only depends on the charge of the native (i.e., nonreduced) HPAs. In other words, the times for both native and reduced forms of a particular HPA are the same. Remarkably, the onset times only increase with the increase in the magnitude of the charge on the native HPAs (from 90 to 170 to 240 s for, in order, P-HPA^{3-}, Si-HPA^{4-}, and Al-HPA^{5-}, see Figure 3). This shows that the crystallization of HPAs is mainly controlled by the most stable oxidation state in solution provided that the crystallization is done by evaporation at ambient conditions. To recap, a correlation between the charge of the HPAs and the liquid-like correlated structures formed at the onset of crystallization is observed in aqueous solutions.

We have also investigated the crystals that formed in the drops by analysis of the sharp Debye–Scherrer rings that appear in the SAXS patterns of Figure 4a–f. The peak positions obtained from all the patterns are shown in Figure 4g. At first

DOI: 10.1021/jacs.5b13375
J. Am. Chem. Soc. 2016, 138, 7282–7288

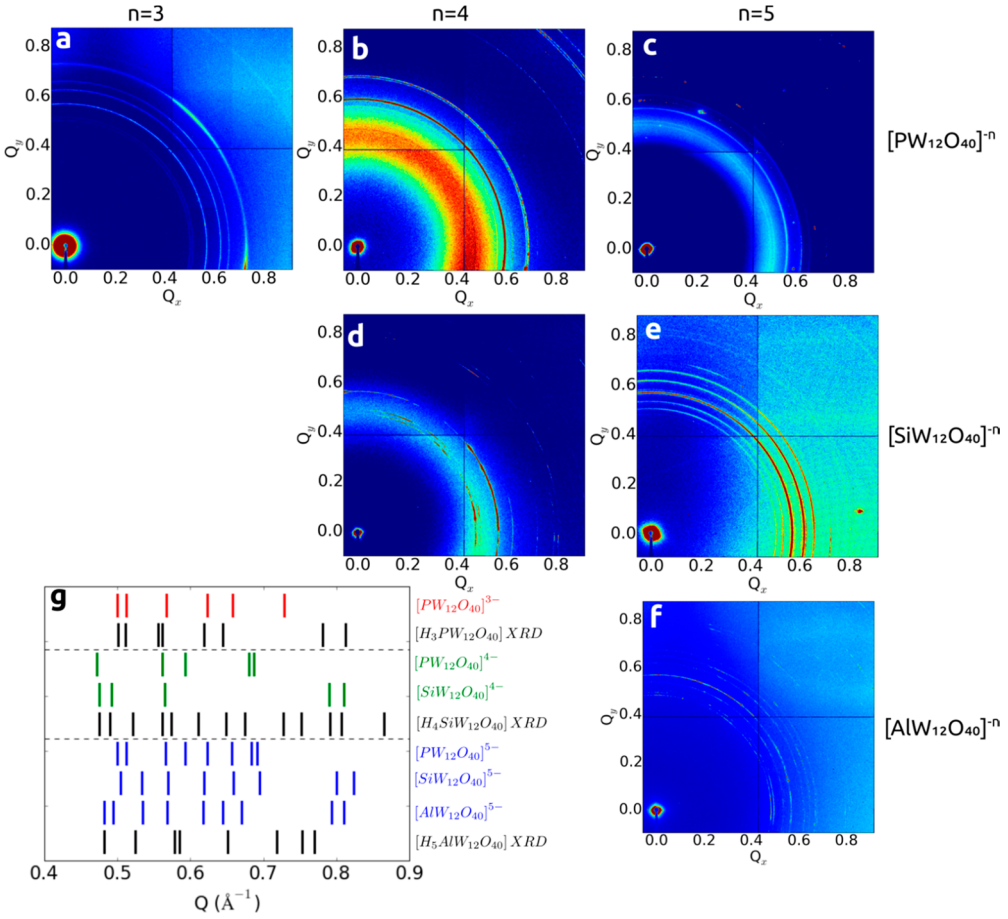

Figure 4. 2D SAXS patterns collected from the dried-out drops of the starting solutions containing 0.4 M $H_nPW_{12}O_{40}$ (a–c), $H_nSiW_{12}O_{40}$ (d and e), and $H_nAlW_{12}O_{40}$ (f) with n = 3–5 showing the Debye–Scherrer rings. (g) Comparison of the peak positions of the Debye–Scherrer rings obtained from the different HPAs (red (n = 3), green (n = 4), and blue (n = 5) vertical lines). The peak positions obtained from the powder XRD data of crystals obtained ex situ by evaporating 0.4 M solutions of $H_3PW_{12}O_{40}$, $H_4SiW_{12}O_{40}$, and $H_5AlW_{12}O_{40}$ in 0.1 M HCl are shown as black vertical lines.

glance, the Bragg peak positions obtained from different HPAs with different charges—native and reduced—appear to be different. However, on closer examination, we find several correlations. On the one hand, the peak positions of the doubly reduced P-HPA^{-5} are a combination of the peak positions for singly reduced P-HPA^{-4} and the native P-HPA^{-3}. On the other, the peak positions of singly reduced P-HPA^{-4} are different from native P-HPA^{-3}; the same is true for singly reduced Si-HPA^{-5} and native Si-HPA^{-4}. In order to determine if the crystals formed within the pendant drop are metastable phases, we obtained the powder X-ray diffraction (XRD) patterns shown in Figure S4 (SI) for the stable equilibrium crystals obtained ex situ by evaporating solutions of native P-HPA^{-3}, Si-HPA^{-4}, and Al-HPA^{-5}. The peak positions obtained from the powder XRD are shown as black solid lines in Figure 4g. Although a few peak positions from the powder XRD patterns of the equilibrium crystals match the positions for the crystals formed in the pendant drops, most of the peak positions do not match. This mismatch suggests that the crystallization of HPAs involves the formation of intermediate metastable polymorphic forms, a behavior that is consistent with Ostwald's rule of stages. We did not witness the transition from the metastable crystalline HPA phases in the pendant drops to the equilibrium crystalline phases in the solid salts mainly due to the fact that, at the end of a complete evaporation cycle, the hanging polycrystalline lumps were not suitable for collecting meaningful diffraction data.

Crystallization of HPAs via a Two-Step Process. As evident from the in situ SAXS data obtained from HPAs with different charges, liquid-like correlated structures are observed in evaporating aqueous solutions as volume is decreased long before the crystallization process starts. The average separation between HPAs in 0.4 M solutions can be estimated from the Wigner–Seitz radius. The result, 20 Å, corresponds to the average separation between the HPAs distributed uniformly and randomly throughout the solution. Apart from the native P-HPA^{-3}, the average HPA–HPA separation, d, obtained for all the HPAs, both native and reduced, is much smaller than 20 Å (see Figure 3). The larger value of d obtained for P-HPA^{-3} (18.0 Å) at the instant of drop formation is due to the fact that the P-HPAs form monomer-percolated structures in solution as reported elsewhere.[40] This indicates that the distribution of HPAs in solution is not uniform; rather, regions with high and low density fluctuations are observed well before reaching the saturation concentration. Although experiments[6,13−17] and simulations[18,19] have revealed such density fluctuations in under-saturated aqueous solutions of organic colloids and proteins beforehand, here we have shown that they also apply to inorganic oxoanions in much the same manner as observed in a recent TEM study of the early stages of crystallization of $CaCO_3$.[5] Our first of the kind experimental observations of

DOI: 10.1021/jacs.5b13375
J. Am. Chem. Soc. 2016, 138, 7282–7288

density fluctuations of HPAs before the onset of crystallization in aqueous solutions are evidence of liquid−liquid phase separation. This phenomenon, which was observed in several previous experiments[6,13−17] and simulations,[18,19] was interpreted as the first step of a two-step process. The most important property of the dense correlated liquid HPA phases is the continuous structural change (manifest in the decrease in d and increase in ξ) as a function of concentration (due to evaporation of the solvent) up to the point of solution saturation. This is a unique behavior. It is not observed for other ions or colloids.

As shown in our recent study[40] on the solution aggregation behaviors of HPAs, the interactions between them are dictated by hydrogen-bonding and Coulomb interactions. These appear to carry over from the solid state wherein stable crystalline structures[41] consist of HPAs that are connected through H-bonded networks. As noted here, the unique solution behaviors of HPAs, in terms of their continuously changing liquid-like structure before the onset of crystallization, suggest the presence of H-bonding networks that play a crucial role in templating correlations between them. In fact, our experimental results show charge-dependent critical values of d and ξ that are diagnostic of the first stage (i.e., correlation) of the crystallization process. In the second stage (i.e., condensation) of the process, when the critical values of d and ξ are reached, crystallization occurs via the formation of metastable polymorphic crystal forms that are in equilibrium with the surrounding dense liquid-like correlated phases. The two-step process is depicted in Figure 2. The first step exhibits continuously changing liquid-like phases of HPAs prior to crystallization. This observation is similar to the first step in the formation of nanoparticles reported by Finke and co-workers.[1,22−24] The second step involves the formation of crystals that transform through different metastable structures before reaching the equilibrium structures after complete drying of the solvent. This step is very fast compared to the first one as evidenced by our observations of very sharp Bragg peaks essentially instantaneously with the onset of crystallization. Once the crystals start forming, they grow very rapidly. This phenomenon is kinetically characterized as catalytic surface growth by Finke et al.[1,22−24]

CONCLUSIONS

By using in situ SAXS measurements, we have shown that Keggin heteropolyanions undergo a two-step process leading to crystallization in aqueous solutions. The first step is the formation of charge-dependent dense liquid-like correlated phases that precedes the second step with the formation of metastable polymorphic crystals in equilibrium with the dense liquid-like phases. In the first step, the dense liquid-like HPA phases continuously evolve with time. The evolution is observed in terms of the decrease in the average separation (d) between the HPA ions and the increase in their correlation lengths (ξ) with solvent evaporation up until the onset of crystallization. In the second step, the dense liquid-phase transforms to crystals; throughout this transformation both d and ξ of the correlated liquid phase remain constant right through to the complete evaporation of the solvent. Once the formation of HPA crystals begins, they grow almost instantaneously and evolve continuously, while in contact with the dense liquid phase, to reach the stable equilibrium phases after completion of the evaporation process. Although our SAXS results for the six HPA systems provide new structural insights into the crystallization behaviors of inorganic ions in solution, the approach does not provide access to mechanistic descriptions of each step that would be available from kinetic studies. In this regard and from a general (i.e., system-independent) perspective, the combination of both metrics, as reported here, and kinetics, as demonstrated elsewhere,[1,22−24,29] is pivotal to access fundamental knowledge about the mechanisms of nucleation, growth, and agglomeration phenomena throughout nature.

EXPERIMENTAL SECTION

Chemicals. The heteropolyacids $H_3PW_{12}O_{40}\cdot 4H_2O$ and $H_4SiW_{12}O_{40}\cdot 4H_2O$ were used as received from Sigma-Aldrich. Hydrochloric acid was procured from Fisher Chemical (Optima). $H_5AlW_{12}O_{40}\cdot 5H_2O$ was synthesized according to the methods of Cowan et al.[42] The waters of hydrations of the heteropolyacids were determined using thermogravimetric analysis. Stock solutions of 0.4 M of each of the three heteropolyacid salts were prepared in 0.1 M HCl aqueous electrolytes. In these, the salts fully dissociate into HPAs ($PW_{12}O_{40}^{3-}$, $SiW_{12}O_{40}^{4-}$, $AlW_{12}O_{40}^{5-}$) and protons (H_3O^+).

Bulk Electrolysis. In order to observe the effect of HPA charge on their crystallization behaviors, we performed controlled-potential (bulk) electrolyses to reduce them by one- and two-electrons. The reduction process provides well-known dark-blue colored heteropolyblues[43] of P-HPA^{4-} (singly reduced P-HPA^{3-}), P-HPA^{5-} (doubly reduced P-HPA^{3-}), and Si-HPA^{5-} (singly reduced Si-HPA^{4-}). The details of the related electrochemical measurements and bulk electrolysis are provided in the SI Section S1.

Pendant Drop SAXS. SAXS data were collected at beamline 12-ID-C at the Advanced Photon Source at Argonne National Laboratory using a custom-built pendant drop system to acquire solution data in a "containerless" fashion. This particular method is used to avoid heterogeneous surface-activated processes and to monitor crystallization in the homogeneous drop. The incident X-ray energy was 28 keV. We started the data acquisition with a pendant drop of 20 μL hanging from a Teflon syringe needle (as shown in Figure 1) for each of the solutions. Under ambient conditions, the solvent (water) of the solution evaporates with time; this evaporation increases the density of the drop until the saturation concentration is reached and crystals start forming. Crystal formation is indicated by the appearance of sharp peaks in the SAXS patterns. In order to keep the drop size constant, a few microliters of stock solution are released from the syringe in an intermittent fashion. We collected SAXS data with a time interval of 10 s between consecutive frames for each solution up until the time that crystal formation was detected. The geometry of the SAXS instrument was optimized to collect data with a maximum scattering momentum (Q_{max}) of 0.9 Å^{-1}. The extraction of the structure factor response ($S(Q)$) from the intensity of the experimental SAXS signal ($I(Q)$) by background subtraction and normalization with the corresponding form factors ($P(Q)$) of the HPA is discussed elsewhere.[40] It is to be noted that due to the intermittent addition of the solution from the reservoir and the diffusion of ions from the needle to the drop or vice versa, it is not possible to track the exact concentration of the drop as a function of time. Due to diffusion, the effective change in the HPA concentration in the evaporating drop will be slower than the condition of no diffusion.

ASSOCIATED CONTENT

Supporting Information

The Supporting Information is available free of charge on the ACS Publications website at DOI: 10.1021/jacs.5b13375.

Details of the bulk electrolysis of the solution, time-dependent SAXS data, and powder XRD patterns of the heteropolyanions (PDF)

DOI: 10.1021/jacs.5b13375
J. Am. Chem. Soc. 2016, 138, 7282−7288

AUTHOR INFORMATION

Corresponding Authors

*mrinal.bera@esrf.fr or nayanbera@gmail.com

*mantonio@anl.gov

Present Address

†DUBBLE-CRG, European Synchrotron Radiation Facility (ESRF), CS40220, 38043 Grenoble Cedex 9, France.

Notes

The authors declare no competing financial interest.

ACKNOWLEDGMENTS

We thank our Argonne colleague Dr. Soenke Seifert for assistance with small-angle X-ray scattering experiments and Dr. Benjamin Burton-Pye (Lehman College) for the synthesis of aluminotungstic acid. This work and the use of the Advanced Photon Source are supported by the U.S. Department of Energy, Office of Science, Office of Basic Energy Sciences, Division of Chemical Sciences, Biosciences and Geosciences, under contract No DE-AC02-06CH11357.

REFERENCES

(1) Watzky, M. A.; Finke, R. G. *J. Am. Chem. Soc.* **1997**, *119*, 10382−10400.

(2) Sleutel, M.; Van Driessche, A. E. S. *Proc. Natl. Acad. Sci. U. S. A.* **2014**, *111*, E546−E553.

(3) Habchi, J.; Arosio, P.; Perni, M.; Costa, A. R.; Yagi-Utsumi, M.; Joshi, P.; Chia, S.; Cohen, S. I. A.; Müller, M. B. D.; Linse, S.; Nollen, E. A. A.; Dobson, C. M.; Knowles, T. P. J.; Vendruscolo, M. *Science Advances* **2016**, *2*, e1501244.

(4) Chung, S.-Y.; Kim, Y.-M.; Kim, J.-G.; Kim, Y.-J. *Nat. Phys.* **2009**, *5*, 68−73.

(5) Nielsen, M. H.; Aloni, S.; De Yoreo, J. J. *Science* **2014**, *345*, 1158−1162.

(6) Vekilov, P. G. *Nanoscale* **2010**, *2*, 2346.

(7) Erdemir, D.; Lee, A. Y.; Myerson, A. S. *Acc. Chem. Res.* **2009**, *42*, 621−629.

(8) Myerson, A. S.; Trout, B. L. *Science* **2013**, *341*, 855−856.

(9) Vorontsova, M. A.; Maes, D.; Vekilov, P. G. *Faraday Discuss.* **2015**, *179*, 27−40.

(10) ten Wolde, P. R.; Frenkel, D. *Phys. Chem. Chem. Phys.* **1999**, *1*, 2191−2196.

(11) Zhang, T. H.; Liu, X. Y. *Angew. Chem., Int. Ed.* **2009**, *48*, 1308−1312.

(12) Gibbs, J. W. *Scientific Papers of J. Willard Gibbs*; Longmans, Green, and Co.: London, 1906; Vol. *1*.

(13) Chowdhury, A. U.; Dettmar, C. M.; Sullivan, S. Z.; Zhang, S.; Jacobs, K. T.; Kissick, D. J.; Maltais, T.; Hedderich, H. G.; Bishop, P. A.; Simpson, G. J. *J. Am. Chem. Soc.* **2014**, *136*, 2404−2412.

(14) Chung, S.-Y.; Kim, Y.-M.; Kim, J.-G.; Kim, Y.-J. *Nat. Phys.* **2009**, *5*, 68−73.

(15) Pienack, N.; Bensch, W. *Angew. Chem., Int. Ed.* **2011**, *50*, 2014−2034.

(16) Schüth, F.; Bussian, P.; Agren, P.; Schunk, S.; Lindén, M. *Solid State Sci.* **2001**, *3*, 801−808.

(17) Zhang, T. H.; Liu, X. Y. *Angew. Chem., Int. Ed.* **2009**, *48*, 1308−1312.

(18) Chakraborty, D.; Patey, G. N. *J. Phys. Chem. Lett.* **2013**, *4*, 573−578.

(19) ten Wolde, P. R.; Frenkel, D. *Science* **1997**, *277*, 1975−1978.

(20) Ostwald, W. *Z. Phys. Chem.* **1897**, *22*, 289−330.

(21) Zhang, T. H.; Liu, X. Y. *J. Phys. Chem. B* **2007**, *111*, 14001−14005.

(22) Laxson, W. W.; Finke, R. G. *J. Am. Chem. Soc.* **2014**, *136*, 17601−17615.

(23) Mondloch, J. E.; Yan, X.; Finke, R. G. *J. Am. Chem. Soc.* **2009**, *131*, 6389−6396.

(24) Watzky, M. A.; Finney, E. E.; Finke, R. G. *J. Am. Chem. Soc.* **2008**, *130*, 11959−11969.

(25) Soga, K. G.; Melrose, J. R.; Ball, R. C. *J. Chem. Phys.* **1999**, *110*, 2280−2288.

(26) Wallace, A. F.; Hedges, L. O.; Fernandez-Martinez, A.; Raiteri, P.; Gale, J. D.; Waychunas, G. A.; Whitelam, S.; Banfield, J. F.; Yoreo, J. J. D. *Science* **2013**, *341*, 885−889.

(27) ten Wolde, P. R.; Frenkel, D. *Phys. Chem. Chem. Phys.* **1999**, *1*, 2191−2196.

(28) Baumgartner, J.; Dey, A.; Bomans, P. H. H.; Le Coadou, C.; Fratzl, P.; Sommerdijk, N. A. J. M.; Faivre, D. *Nat. Mater.* **2013**, *12*, 310−314.

(29) Finney, E. E.; Finke, R. G. *Chem. Mater.* **2009**, *21*, 4692−4705.

(30) Sear, R. P. *J. Phys.: Condens. Matter* **2007**, *19*, 033101.

(31) Jeannin, Y. P. *Chem. Rev.* **1998**, *98*, 51−76.

(32) Ammam, M. *J. Mater. Chem. A* **2013**, *1*, 6291−6312.

(33) Kourasi, M.; Wills, R. G. A.; Shah, A. A.; Walsh, F. C. *Electrochim. Acta* **2014**, *127*, 454−466.

(34) Kozhevnikov, I. V. *Chem. Rev.* **1998**, *98*, 171−198.

(35) Liu, T. B.; Diemann, E.; Li, H. L.; Dress, A. W. M.; Muller, A. *Nature* **2003**, *426*, 59−62.

(36) Yin, P.; Li, D.; Liu, T. *Chem. Soc. Rev.* **2012**, *41*, 7368−7383.

(37) Verhoeff, A. A.; Kistler, M. L.; Bhatt, A.; Pigga, J.; Groenewold, J.; Klokkenburg, M.; Veen, S.; Roy, S.; Liu, T.; Kegel, W. K. *Phys. Rev. Lett.* **2007**, *99*, 066104.

(38) Antonio, M. R.; Nyman, M.; Anderson, T. M. *Angew. Chem.* **2009**, *121*, 6252−6256.

(39) Pigga, J. M.; Kistler, M. L.; Shew, C.-Y.; Antonio, M. R.; Liu, T. *Angew. Chem., Int. Ed.* **2009**, *48*, 6538−6542.

(40) Bera, M. K.; Qiao, B.; Seifert, S.; Burton-Pye, B. P.; Olvera de la Cruz, M.; Antonio, M. R. *J. Phys. Chem. C* **2016**, *120*, 1317−1327.

(41) Brown, G. M.; Noe-Spirlet, M. R.; Busing, W. R.; Levy, H. A. *Acta Crystallogr., Sect. B: Struct. Crystallogr. Cryst. Chem.* **1977**, *33*, 1038−1046.

(42) Cowan, J. J.; Hill, C. L.; Reiner, R. S.; Weinstock, I. A. *Inorg. Synth.* **2002**, *33*, 18−26.

(43) Pope, M. T. *Heteropoly and Isopoly Oxometalates*; Springer-Verlag: Berlin, 1983; Vol. *8*.

DOI: 10.1021/jacs.5b13375
J. Am. Chem. Soc. 2016, 138, 7282−7288